Journal of Molecular Liquids 320 (2020) 114492

Contents lists available at ScienceDirect

Journal of Molecular Liquids

journal homepage: www.elsevier.com/locate/molliq

Correlation between adhesion strength and phase behaviour in solid-supported lipid membranes

N. Bibissidis [a], K. Betlem [a], G. Cordoyiannis [b], F. Prista-von Bonhorst [a], J. Goole [c], J. Raval [d], M. Daniel [b], W. Góźdź [d], A. Iglič [e], P. Losada-Pérez [a,*]

[a] Experimental Soft Matter and Thermal Physics (EST) Group, Department of Physics, Université Libre de Bruxelles, Boulevard du Triomphe CP223, 1050 Brussels, Belgium
[b] Faculty of Mechanical Engineering, Czech Technical University in Prague, Technická 4, 16000 Prague 6, Czech Republic
[c] Laboratory of Pharmaceutics and Biopharmaceutics, Université libre de Bruxelles, Campus de la Plaine, CP 207, Boulevard du Triomphe, Brussels 1050, Belgium
[d] Institute of Physical Chemistry, Polish Academy of Sciences, Kasprzaka 44/52, 01-224 Warsaw, Poland
[e] Laboratory of Physics, Faculty of Electrical Engineering, University of Ljubljana, Tržaška 25, Ljubljana, Slovenia

ARTICLE INFO

Article history:
Received 27 July 2020
Received in revised form 25 September 2020
Accepted 1 October 2020
Available online 8 October 2020

Keywords:
Solid-supported lipid membranes
Vesicle adhesion
Quartz crystal microbalance with dissipation
Phase transitions

ABSTRACT

Fundamental understanding of vesicle adhesion in the size range ≤ 200 nm is of major importance when addressing biologically relevant processes involving the presence of small vesicles like exosomes or endosomes. Using quartz crystal microbalance with dissipation monitoring, we investigate the correlation between vesicle deformation and eventual membrane rupture on surfaces with different adhesion levels, as well as their respective thermotropic phase transitions. In particular, phase transitions of solid-supported membranes on Au resemble the cooperative behaviour of lipid membrane transitions in bulk. In contrast, solid-supported membranes on SiO_2 exhibit broadened 'double-peak' transitions, rendering a 'decoupling' effect during melting due to stronger interactions with SiO_2. This paper provides a comprehensive view of the correlation between size, geometry and phase transitions observed in the layer of adsorbed lipid vesicles/membranes. It paves the way to explore structural changes on more complex biointerfaces by acoustic-based sensors.

1. Introduction

Lipid vesicles are self-assembled structures customarily used as model systems for cell membrane basic studies [1,2], as nanocontainers for bio-reactions [3] and in biotechnology applications such as drug delivery or biosensors [4,5]. When supported on solid-surfaces, they might form intact supported vesicle layers (SVLs) or eventually rupture into planar supported lipid bilayers (SLBs). The latter are the result of spontaneous adsorption of small (diameter ≤ 200 nm) vesicles onto solid surfaces. The geometry of SVLs captures the volume to area ratio of the vesicles, strength of adhesion, membrane bending properties and osmotic stress within the supported layer making SVLs useful biomimetic platforms to probe membrane deformation. The latter plays an important role in biological processes such as adhesion, budding, lipid membrane exchange, fission and fusion [6–8]. SVLs are mimics to endosomes or exosomes, which are important for chemical transport and intercellular communication [9,10]; however, these systems are optically inaccessible and the experimental investigation of their deformation is not straightforward. Adsorbed vesicles onto inorganic surfaces serve also as model systems relevant to biocompatibility studies. The shape of a vesicle upon adsorption to a surface is determined by the interplay of adhesion, bending and geometrical constraints. This interplay is theoretically studied starting from a simple model in which the membrane experiences a contact potential arising from the attractive surface. Let us recall the free energy F expression of an adsorbed vesicle in terms of a simple model taking into account the adhesion energy, the local bending energy term and the geometrical constraints [6,11]:

$$F = \frac{1}{2}\kappa \oint (C_1 + C_2 - C_0)^2 dA + \kappa_G \oint C_1 C_2 dA - W A_c + PV + \Sigma A. \quad (1)$$

The first two terms depend on the local bending modulus κ, on the Gaussian curvature modulus κ_G and on C_1, C_2, and C_0 denoting the two principal curvatures, and the (effective) spontaneous curvature, respectively, and dA being an infinitesimal membrane area element. The third term is the adhesion free energy with W being the strength of adhesion and A_c the contact area of the membrane and the surface. The last two terms represent the volume (V) and area (A) constraints with corresponding Lagrange multipliers P and Σ.

Vesicle deformation upon adhesion depends strongly on the lipid organization of the vesicle membrane, which in turn is intimately linked to their phase behaviour [12–15]. The study of vesicles within such a small size range typically requires surface-sensitive techniques, since

* Corresponding author.
E-mail address: plosadap@ulb.ac.be (P. Losada-Pérez).

https://doi.org/10.1016/j.molliq.2020.114492

vesicles with diameter ≤ 200 nm are optically inaccessible structures. Moreover, the study of these phenomena by traditional calorimetric approaches is often hindered by the instability of SUV dispersions, which tend to fuse into larger LUVs and sediment over long-term measurements [16,17].

In this context, quartz crystal microbalance with dissipation monitoring (QCM-D) has recently emerged as a versatile technique to detect and characterize phase transformations of solid-supported lipid membrane geometries, namely SLBs and SVLs [18]. QCM-D is an acoustic-based, label-free technique used extensively in bio-interfacial science and has particularly contributed to the understanding of the kinetics of adsorption and formation of supported lipid bilayers [19–22] and probing their interactions with relevant biomolecules [23,24]. QCM-D is highly sensitive to mass and energy dissipation changes at the solid-lipid layer-liquid interface. In the particular case of adsorbed vesicles, it can detect changes in their geometry (shape) and membrane conformation when these systems undergo phase transitions [25–27]. In this work we address the question whether and how the supported membrane shape affects the phase transitions in solid-supported membranes. Vesicles of dipamitoylphosphatidylcholine (DPPC) are chosen, since DPPC is a saturated phospholipid ubiquitous in eukaryotic cells and a well-known lung surfactant, whose main phase transition is well-characterized in bulk [28,29]. Two solid surfaces bearing different adhesion levels are used, polycrystalline Au, an interesting transducer material owing to its good thermal and electrical conductivities, plasmon resonance and biocompatibility [30], and SiO_2 which bears a negative charge and additional electrostatic interactions [31–33] in determining adhesion [34,35]. The correlation between surface wettability and membrane phase transitions has been explored as a function of vesicle size and adsorption temperature. Numerical calculations based on free energy minimization of Eq. (1) provide complementary information on the adsorbed vesicle systems.

2. Materials and methods

2.1. Materials

DPPC lipid was purchased from Avanti Polar Lipids (Alabaster, AL) and spectroscopic grade chloroform from Analar (Normapur). Dioodomethane (≥98.5%) was purchased from Merck. HEPES buffer (pH 7.4) consisting of 10 mM HEPES (99%) and 150 mM NaCl, both from Sigma-Aldrich (≥99.5%) was utilized for hydration of the dried lipid films. The quantities of lipids were determined gravimetrically using an analytical balance (AG245, Metter-Toledo, Switzerland) with a precision of ±0.1 mg.

2.2. Vesicle preparation

DPPC lipid in powder form was first dissolved in spectroscopic grade chloroform, and the solvent was evaporated under a mild flow of nitrogen in a round bottomed flask. The lipid film was kept under low pressure overnight to remove any traces of remaining solvent. The film was then hydrated with HEPES buffer to 1 mg/mL under continuous stirring in a temperature-controlled water bath at 55 °C (well above the melting temperature of DPPC T_m ~ 41.5 °C). Large unilamellar vesicles (LUVs) and small unilamellar vesicles (SUVs) were formed by extrusion through filters with different pores sizes (100 nm or 30 nm) for a fixed number of passes. LUVs were formed after 25 passes through a 100 nm-pore filter, while SUVs were formed after 25 passes through a 100 nm-pore filter followed by 15 passes through a 30 nm-pore filter.

2.3. Dynamic light scattering

Vesicle effective sizes and polydispersity were determined by dynamic light scattering (DLS) (Malvern Zetasizer Nano ZS, Malvern, UK). The obtained mean diameters and polydispersity indexes of the samples used are displayed in Table 1.

Table 1
Hydrodynamic mean diameters and polydispersity indexes (PI) obtained by DLS for the DPPC vesicle dispersions used in this work. The number of performed measurements per sample is $n = 4$.

Type of vesicles	Mean diameter (nm)	PI
LUVs	138 ± 40	0.10
SUVs	72 ± 25	0.07

2.4. Quartz crystal microbalance with dissipation monitoring (QCM-D)

A Qsense E4 instrument (Gothenburg, Sweden) monitoring the frequency and dissipation changes, Δf and ΔD was used. Q-sense E4 also enables heating or cooling temperature scans in the range between 15 °C and 65 °C. AT-cut quartz crystals with Au and SiO_2 coating (diameter 14 mm, thickness 0.3 mm, quoted surface roughness < 3 nm, and resonant frequency 4.95 MHz) were used. The Au-coated quartz sensors were cleaned with a 5:1:1 mixture of Milli-Q water (resistance of 18.2 MΩ cm at 25 °C), ammonia and hydrogen peroxide, and were UV-ozone treated with a UV-ozone cleaner (Bioforce Nanosciences, Germany) for 20 min, followed by rinsing in Milli-Q water and drying with N_2. SiO_2-coated quartz sensors were cleaned in a solution of sodium dodecyl sulfate (2% SDS) for several hours and UV-ozone treated for 20 min, followed by rinsing in Milli-Q water and drying with N_2. The changes in Δf/n and in ΔD were monitored at four different overtones (from 3rd to 9th). The lipid vesicles were inserted into the QCM-D cells with a flow rate of 50 μL/min. Vesicle adsorption experiments were carried out at two different temperatures, at 16 °C and at 50 °C, where DPPC is in phases possessing different bending rigidities, the gel phase and the liquid-disordered phase, respectively. The temperature stability is in the order of ±0.02 °C around the set value. First, a baseline with pure HEPES buffer was established and afterwards lipid vesicles were injected over the Au-coated or SiO_2-coated sensor chips. After reaching a stable supported membrane layer the pump was switched off and the ensemble was left to stabilize for several hours. Subsequent temperature scans, upon heating and cooling, were performed at a rate of 0.4 °C/min, maintaining a 60 min stabilization time between successive temperature ramps. Measurements were repeated at least three times to check the reproducibility of the results.

2.5. Contact angle measurements

Contact angle (CA) measurements were carried out using an Attension ThetaLite from Biolin Scientific (Sweden) based on the sessile drop method. A small drop (3 μL) of Milli-Q water or diiodomethane was deposited onto clean, UV-ozone treated Au-coated or SiO_2 quartz surfaces, and the shape of the drop formed on the surface was analysed. The contact angle of the 3 μL droplet of either ultrapure water or diiodomethane was determined over a time period of 10 s using a recording speed of 20 frames/s and, afterwards, the average of several drops was calculated. The CA was measured at several points, and an average value was extracted. All contact angles were measured at a room temperature. Surface free energies of UV-ozoned Au and SiO_2 surfaces γ_{sv} (polar γ_{sv}^p and dispersive γ_{sv}^d parts) were determined based on the

Table 2
Contact angle data acquired with two liquids, water and diiodomethane (DI), and calculated surface energies for the solid surfaces under study.

Sample	θ_{water} (°)	θ_{DI} (°)	γ_{sv} (mN/m)	γ_{sv}^d (mN/m)	γ_{sv}^p (mN/m)
Au	38 ± 4	20 ± 2	66 ± 4	48 ± 3	19 ± 2
SiO_2	10 ± 1	42.3 ± 0.5	74 ± 2	38.4 ± 0.5	35 ± 1

Owens, Wendt, Rabel and Kaelble method [36] and are included in Table 2. Details on calculations are included in the Supplementary material.

3. Results and discussion

3.1. Vesicle adsorption and layer formation

Fig. 1 shows the Δf and ΔD responses (represented for the third overtone) during vesicle adsorption and supported lipid layer formation on SiO_2 and Au at temperatures well below (16 °C) and above (50 °C) the melting temperature of DPPC. The mechanistic scenario of the observed Δf and ΔD changes is governed by a delicate balance between the adhesive energy from lipid-surface interactions (which tends to maximize the contact area between the vesicle membrane and the surface) and the opposing effect of bending the bilayer [37].

When adsorbed onto Au, a monotonic frequency decrease (mass increase) and dissipation increase can be observed reaching constant non-zero Δf and ΔD plateau values. Such time-dependent responses provide evidence that oxidized Au facilitates non-ruptured vesicle adsorption towards the formation of acoustically non-rigid vesicle layers with saturated coverage.

Although the vesicle adsorption profiles are similar for small and large vesicles when adsorbed in both the gel and liquid disordered phases, it is worth exploring the size- and temperature-dependent differences. After initial adsorption both Δf and ΔD plateau values clearly increase (in absolute value) with increasing vesicle size. For LUVs on Au at $T < T_m$, an overshoot behaviour was observed in the dissipation signal but not on the frequency signal. This peak has been seen in previous works and was ascribed to vesicles 'rocking and rolling motion' [38].

Larger vesicles carry more trapped aqueous buffer (larger frequency shifts) and thus are softer structures (larger dissipation shifts). When adsorbed at $T > T_m$ the same trend with vesicle size was observed, although the plateau values were significantly smaller. At $T < T_m$ the DPPC bilayer envelope of the adsorbed vesicles is in the gel phase and its bending modulus $\kappa \sim 10 \cdot 10^{-19}$ J [39] renders the vesicle membrane more stiff. Above T_m, the bilayer is in the liquid disordered phase and the modulus attains about a ten times smaller value of $\kappa \sim 1 \cdot 10^{-19}$ J. This makes the membrane of vesicles softer and more deformable upon adsorption with larger contact area, yielding a smaller number of vesicles for similar surface coverage.

When adsorbed onto SiO_2, a completely different pattern of behaviour is observed below and above T_m. At $T < T_m$, monotonic frequency and dissipation changes take place reaching constant non-zero Δf and ΔD plateau values. The plateau values follow the same trend with vesicle size as observed in the case of Au. However, the reached plateau values are smaller on SiO_2, indicating that the stronger SiO_2 adhesion might favour vesicle deformation, induce the formation of transient pores [40], local vesicle rupture events and formation of small bilayer patches (from the ruptured vesicles). It is worth noting that QCM-D is very sensitive to hydrodynamic (wet) mass and the local, partial formation of SLBs might be masked by the adsorption of vesicles on top or in between the bilayer patches [41]. At $T > T_m$ an initial monotonic adsorption of vesicles is observed until a critical surface coverage is reached (minimum in Δf and maximum in ΔD), followed by vesicle fusion and rupture to form SLB [21,22,37,41]. The surface-vesicle interactions on SiO_2 are stronger than on Au and the SiO_2-adsorbed vesicles deform to a greater extent with higher contact area and higher membrane lateral tension, making them more prone to pore formation or rupture and fusion [42] and therefore less stable. Note that lipid bilayers in the gel phase can sustain higher lateral tensions and therefore rupture appears at higher values of critical tension (i.e. lysis tension) [43].

Au has been oxidized thus is highly hydrophilic and its isoelectric point is around 4.5 to 5 [44]. The isoelectric point of SiO_2 is around 2.5 [45], therefore both Au and SiO_2 are negatively charged at the current experimental conditions (pH = 7.4), SiO_2 being even more than Au. This confers Au and SiO_2 an attractive potential to support intact vesicles of zwitterionic lipids such as DPPC. The lateral tension arising by attractive forces between the adsorbing vesicles and the surface does not exceed the threshold for permanent membrane rupture in the case of Au.

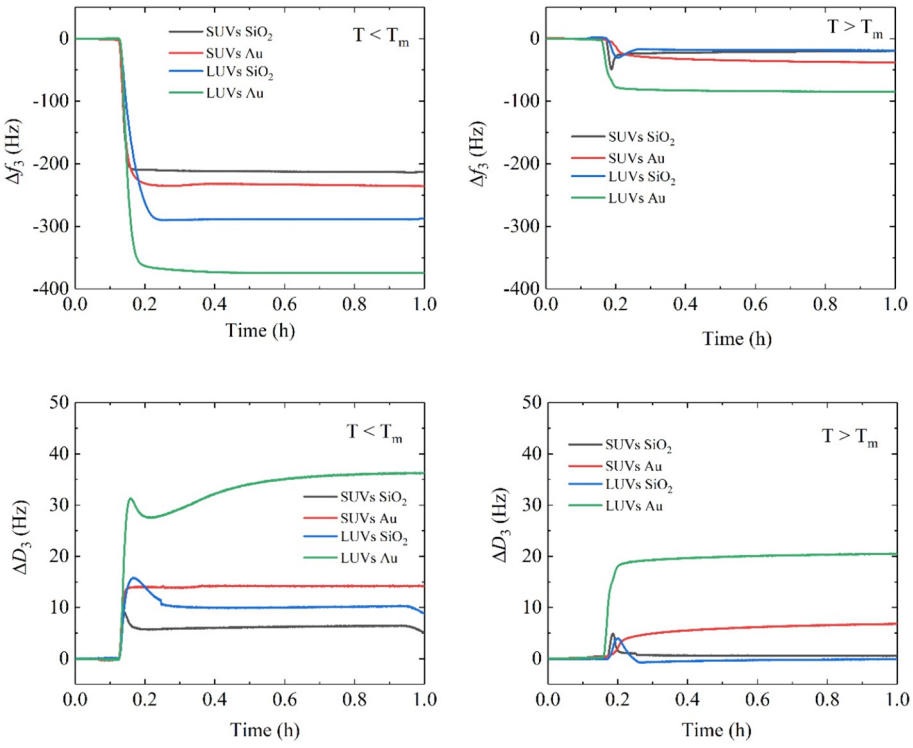

Fig. 1. Left column: the frequency (top panel) and dissipation shifts (bottom panel) are shown for vesicles adsorbed at 16 °C. Right column: the corresponding frequency (top panel) and dissipation shifts (bottom panel) are shown for vesicles adsorbed at 50 °C. Black colour: SUVs on SiO_2; red colour: SUVs on Au; blue colour: LUVs on SiO_2; green colour: LUVs on Au.

As a matter of fact, the polar component of the surface free energy in Au is half the value calculated for SiO_2 (see Table 2), while the dispersive component is larger, in agreement with the large Hamaker constant of Au [46]. In addition, the formation of transient membrane pores [40] cannot be excluded, especially at $T > T_m$, since in the liquid disordered phase the lipid bilayer area stretching modulus is 3 to 4 times smaller than in the gel phase [47]. The theoretically predicted attraction of zwitterionic vesicles (PC headgroup) to negatively charged surfaces (Au or SiO_2) is accompanied by more perpendicular average orientation of the zwitterionic head groups [31–33], i.e. to more tightly packed lipids, which may favour the gel phase of lipids in the adhered part of the vesicle membrane.

The extent of vesicle deformation upon adsorption was estimated following the approach introduced by Tellechea et al. [38]. This method consists in plotting $-\Delta D/\Delta f$ ratio vs $-\Delta f$ for all overtones during initial adsorption (low vesicle surface coverage), which typically shows a linear decrease over a large range of frequency shifts. Extrapolation of this linear decrease to a frequency-independent intercept with the $-\Delta f$ axis (where overtones intersect) provides a value of the thickness of the adsorbed vesicle layer h referred to as Sauerbrey thickness: $h = -\Delta f C/\rho$, where $C = 18$ ng/cm^2 Hz and $\rho = 1$ g/cm^3 is the density of the film [44]. This approach assumes a complete surface coverage at the end of the adsorption process, where the presence of trapped buffer has been diminished to occupy only the void spaces between densely packed vesicles (the $-\Delta D/\Delta f$ ratio is close to zero and the $-\Delta f$ intercept values were the same on the extrapolation of a linear regression) [38,48,49]. Though this approach might not provide a correct absolute value of the real thickness it provides valuable qualitative information. Fig. 2 displays the extrapolated Sauerbrey thickness for LUVs adsorbed at 16 °C and 50 °C onto SiO_2 and Au surfaces. The corresponding figure for SUVs adsorbed at 16 °C and 50 °C onto SiO_2 and Au surfaces is included as Fig. S1 in the Supplementary material.

Sauerbrey layer thickness data are included in Table 3 and it is noteworthy that the obtained values are systematically smaller than those obtained for vesicles in bulk by DLS measurements. For LUVs and SUVs ruptured on SiO2 at $T > T_m$, the thickness obtained are 28 nm and 23 nm, respectively, and this overestimation is likely related to the fact that layers are not fully homogeneous and they might bear some degree of oligolamellarity, especially in the case of ruptured LUVs. The $-\Delta f$ intercept values have been obtained from the average of four overtones. From the Saurbrey thickness values, the extent of vesicle deformation Δd (in percent) was calculated as the relative change of size upon adsorption as compared to the original size of vesicles dispersed in buffer, $\Delta d = \frac{(d_{DLS}-h)}{d_{DLS}} \times 100$. In Fig. 3, the extent of vesicle deformation is displayed for all cases.

The time-independent ΔD vs Δf curves provide additional information on the structural properties of the vesicle adsorbed layers as a function of vesicle size and temperature, reflecting the interplay between bending, adhesion and steric contributions in the vesicle adsorption process. The ΔD–Δf curves in Fig. 4 exhibit steeper slopes with increasing vesicle size, indicating a larger increase in energy dissipation per adsorbing vesicle. At $T > T_m$, LUVs vesicles are prone to larger deformation and are less efficiently packed (so-called steric effect) [50], resulting in a greater viscoelastic contribution per adsorbing vesicle both on Au and SiO_2, the dissipation being smaller in the latter as a result of an increased adhesion interaction and lateral tension by the SiO_2 surface. When adhered onto SiO_2, the fate of adsorbed vesicles depends strongly on temperature; intact but less dissipative vesicle layers are formed as compared to Au at $T < T_m$, while a re-entrant behaviour in the ΔD–Δf curves is observed at $T > T_m$. This results from the combination of three factors i) the increased lateral tension with increased surface adhesion, ii) the decreased bilayer bending modulus and iii) decreased critical tension for rupture upon increasing temperature, resulting in an easier vesicle fusion and rupture.

Table 3
Sauerbrey thickness h and corresponding extent of vesicle deformation Δd values.

		Sensor	h (nm)	Δd (%)
T = 16 °C	LUVs	Au	99 ± 5 nm	28 ± 1
		SiO_2	62 ± 9 nm	58 ± 7
	SUVs	Au	62 ± 4 nm	4 ± 3
		SiO_2	52 ± 4 nm	31 ± 6
T = 50 °C	LUVs	Au	88 ± 11 nm	36 ± 8
		SiO_2	28 ± 3 nm	84 ± 4
	SUVs	Au	50 ± 6 nm	30 ± 7
		SiO_2	23 ± 4 nm	68 ± 6

3.2. Calculations of vesicle shapes upon adsorption

Fig. 5 shows the axisymmetric shapes of the adsorbed vesicles corresponding to minimal free energy given by Eq. (1). In order to better illustrate the effect of the different contributions involved in vesicle adhesion, the vesicle shapes have been calculated for values of reduced volume $v = 6\pi^{1/2}V/A^{3/2}$ [11,51] and parameter $w = WR_s^2/\kappa$, covering a broad range, namely $v = 0.54$, 0.75, 0.85, 0.95 and $w = 0.4$, 6.4, 64 and 640. A detailed description of the numerical procedure for the determination of the vesicles shapes [52] is included in the Supplementary material. For a constant value of the reduced volume v, the calculated shapes depend on the competition between the bending and adhesion contributions. At large w adhesion dominates and favours a large contact area. At small w the obtained shapes of free (non-adhered) membrane parts of the vesicles are more undulated (Fig. 5A and B), since adhesion is smaller and the bending energy takes over. Conversely, at large w, the shapes of the free non-adhered membrane parts become increasingly more spherical (Fig. 5C and D) to maximize the contact area, i.e., the shapes at large w resemble more and more a part of the spherical surface. For very large w (small bending modulus, large W and large

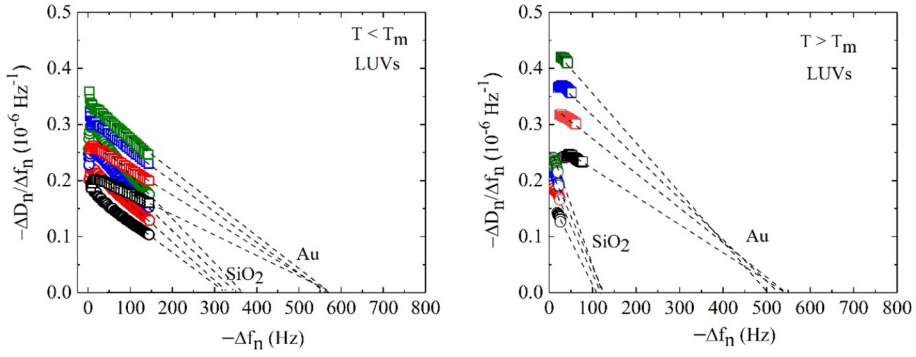

Fig. 2. The $-\Delta D_n/\Delta f_n$ ratio plotted as a function of frequency is presented at different overtones for LUVs onto Au and SiO_2. Left and right panels correspond to vesicles adsorbed at 16 °C and 50 °C, respectively. Data symbols: 3rd overtone (black), 5th overtone (blue), 7th overtone (green), 9th overtone (red).

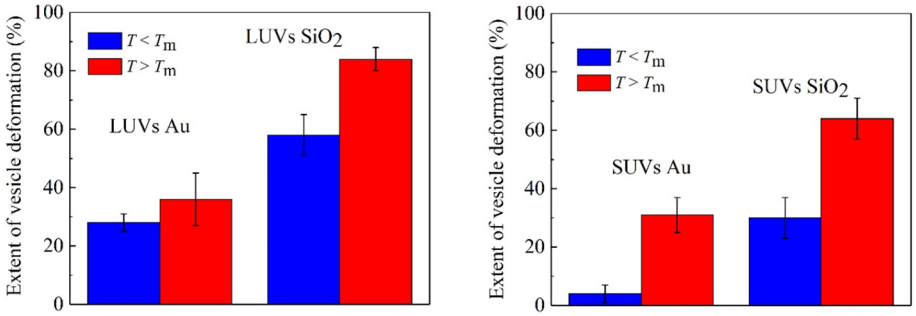

Fig. 3. Extent of vesicle deformation upon adsorption on Au and SiO2 surface above and below the melting temperature of LUVs (left panel) and SUVs (right panel). The red colour corresponds to vesicles adsorbed above melting and blue to the ones below melting.

vesicles) the shapes of the adhered vesicles approach the limiting shape composed of free (non-adhered) part of the membrane which is spherical, and another flat adhered part (Fig. 5D). As it can be seen in Fig. 5D, the limiting shapes depend only on the value of the reduced volume v [53]. The largest part of the vesicle mass and volume is in this case distributed closer to the sensor surface. The obtained nearly limiting shapes for very large values of w (strong adhesion limit) are predominantly determined by the tendency of the vesicles to achieve the maximal possible reduced contact area between the vesicle membrane and the surface (A_c/A) at given reduced volume v. In this regime the influence of the bending energy is very weak and the limiting shapes would be the same also for the initially weakly adsorbed prolate vesicle shapes. It is worth noting that QCM-D experiments were carried out at a rather large vesicle concentration thus the packing efficiency of adhered vesicles and the vesicle contact area can be reduced due to steric effects [50].

In order to better visualize the adhesion strength W behind the results presented in Fig. 5, we have calculated $W = w\kappa/R_s^2$ for $\kappa \sim 10 \cdot 10^{-19}$ J at room temperature (i.e. in the gel phase) and for two values of R_s: 70 nm (LUVs) and 30 nm (SUVs), relevant to this work. For $w = 64$ (corresponding to the shapes of panel C in Fig. 5) we obtain the values $W \sim 15$ mN/m (LUVs) and $W \sim 70$ mN/m (SUVs), corresponding to the range of measured surface energies of water on Au and SiO_2 surfaces given in Table 2.

The first (local bending) energy term in Eq. (1) is scale invariant for $C_0 = 0$ [11], i.e., it is not dependent on the size of the vesicle. Since the second (adhesion) energy term in Eq. (1) is not scale invariant, it becomes increasingly more important for larger vesicles, i.e. larger w since parameter w is proportional to R_s^2 (see also Eq. (12) in Supplementary material). As a consequence, the adhesion is more probable and energetically favourable for larger vesicles. Thus, the size of the vesicle plays an important role in the process of vesicle adhesion, as shown also in the experiments presented in this work (Table 3). The parameter w is proportional to R_s^2 making LUVs more prone to adhere on the larger contact area and deform more. Their shape is closer to the limiting shape not only because they are larger, but also because they are strongly adhered (see Fig. 5D). The parameter w is on other hand inversely proportional to the bending modulus κ and since κ is smaller for $T > T_m$, adhesion becomes stronger for $T > T_m$ and the vesicles shapes are closer to limiting shapes (see Fig. 5D). Moreover, w is larger for SiO_2 surface than for Au because of the larger strength of adhesion W of the SiO_2 surface.

At constant reduced volume v the thickness (height) of the adhered vesicles should be increasing with w for large values of v (see Fig. 5). However, this effect was not observed in the QCM-D experiments for the surface with the largest adhesion strength SiO_2. Indeed, on the SiO_2 surface the reduced vesicle volume v is decreased most likely due to the formation of transient pores [40,54] and/or increase of the vesicle area due to membrane "hidden" pool of lipids, conserved in the form of membrane nanotubular protrusions [55], which is released due to increased membrane lateral tension in the strong adhesion regime. Regarding the formation of the transient pores, it is more plausible to think that they are formed at $T > T_m$. This is because in the liquid disordered phase the lipid bilayer area stretching modulus is smaller than in the gel phase [47] and the lipid bilayer can sustain also lesser critical lateral tension [43] needed for the membrane rupture and formation of transient pores. Accordingly, it can be seen in Table 3 that the thickness h of the adhered vesicles is substantially decreased at $T > T_m$, and, as expected, the effect is more pronounced for the SiO_2 surface.

3.3. Phase transitions

Fig. 6 shows an overview of the temperature dependence of the first-order derivative of Δf shifts (3rd overtone) upon the first heating run for all LUVs and SUVs vesicles adsorbed at $T < T_m$ and $T > T_m$ on Au and SiO_2 surfaces. Upon heating, lipid bilayers change from a stiffer gel phase to a

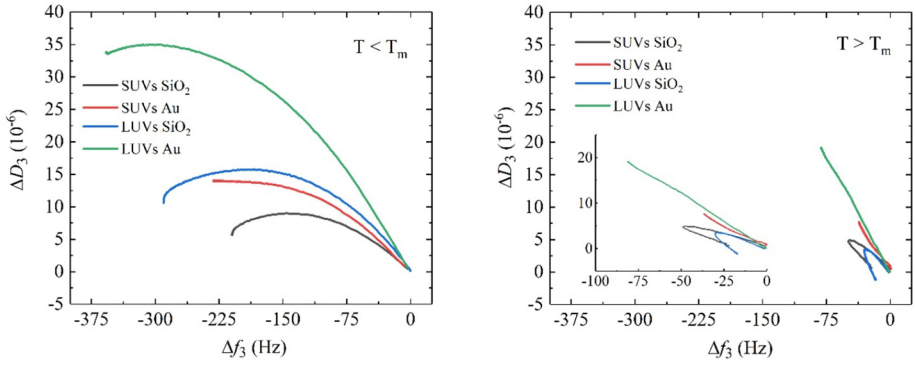

Fig. 4. Comparison between adsorption of vesicles of different sizes onto Au-coated and SiO_2-coated quartz sensors at 16 °C (left panel) and 50 °C (right panel). The same scale is used in both figures for comparison, whereas the inset in the right panel shows a closer view of the ΔD_3-Δf_3 plot for vesicles adsorbed at $T > T_m$.

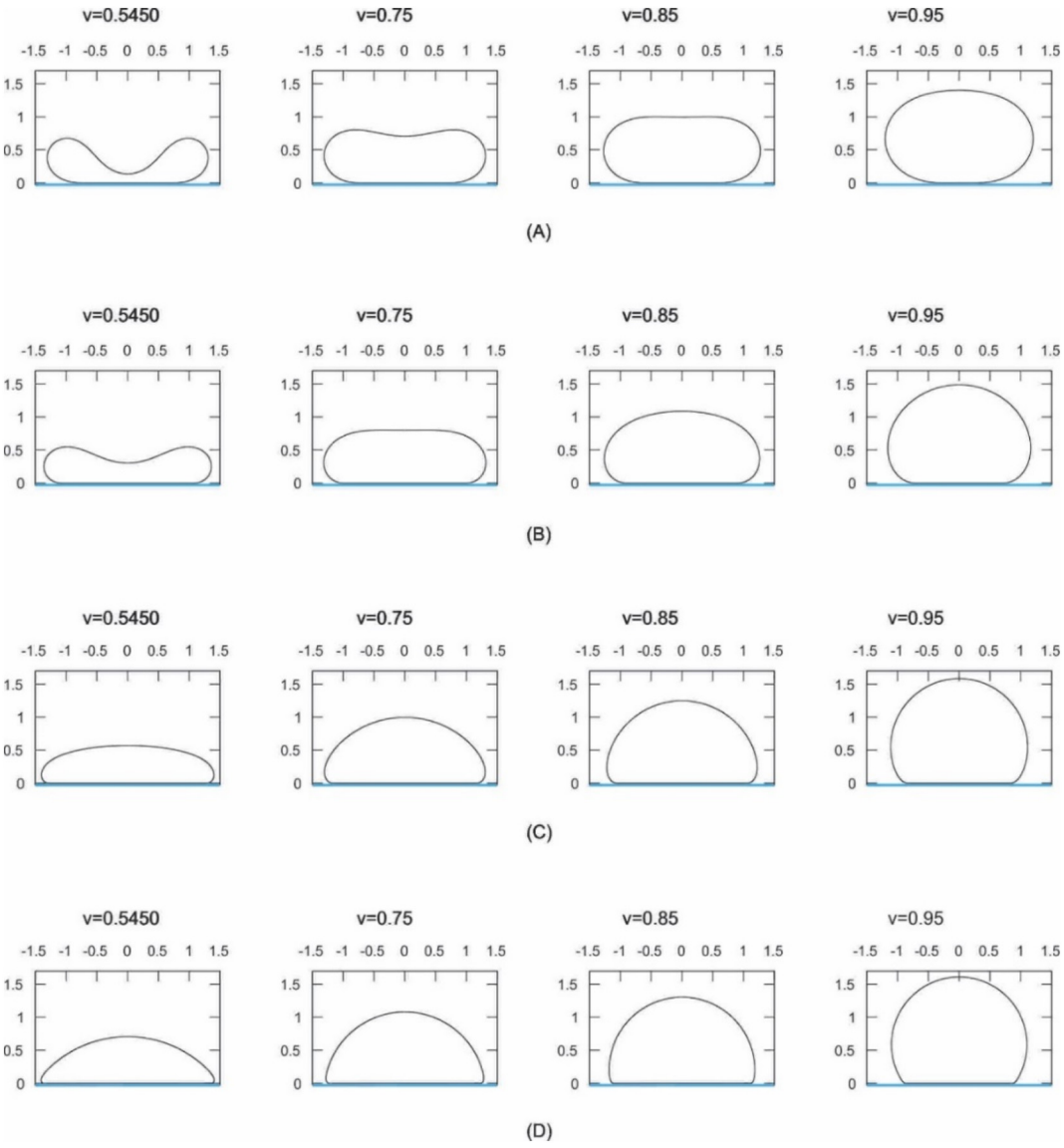

Fig. 5. The shapes of the adsorbed oblate vesicles obtained by the minimization of the free energy given by Eq. (1), determined for different values of reduced volume v and parameter w. Each row represents a different value of w: 0.4 (row A), 6.4 (row B), 64 (row C) and 640 (row D). The spontaneous curvature C_0 was selected to be zero. The calculated shapes of non-adsorbed vesicles corresponding to $w = 0$ and the same reduced volumes v are shown in Fig. S10 of the Supplementary material.

softer liquid-disordered phase. As shown in recent works [18,25–27], these changes are reflected as anomalies in both frequency and dissipation shift signals and, in particular, in their first-derivatives with respect to temperature that display clear extrema. The anomalies are governed by the interplay between changes in thickness, stiffness and, in the case of large adsorbed vesicles, by the presence of hydrodynamic channels, which change the shape of the adsorbed vesicles [26].

The shape of the $d\Delta f(T)/dT$ obtained from QCM-D measurements is reminiscent of that of the isobaric heat capacity $C_p(T)$ from calorimetry during a melting transition [29,56]. In this respect, it is instructive to draw an analogy between these two well-differentiated experimental techniques. Calorimetry is well-established and based on changes in thermal properties when vesicles undergo a phase transition, in this case, the main transition (heat absorption or release). On the other hand, QCM-D is based on changes in the viscoelastic properties of adsorbed vesicles as a result of changes in bilayer thickness, rigidity and vesicle shape. The calorimetric signal yields a maximum in C_p corresponding to a finite jump in enthalpy $H(T)$ along the first order lipid melting transition. The size of this jump scales in this case with the mass; the larger the mass, the larger the heat absorbed or released. In order to draw conclusions on the size of the anomalies observed in $d\Delta f(T)/dT$ let us comment different aspects of Fig. 6 regarding surface free energy, vesicle size and adsorption temperature.

3.3.1. Main phase transition of SVLs on Au surfaces

We start by supported vesicle layers formed on Au exposed to UV-ozone, where no global rupture of vesicles to form SLBs was observed. The main transition appears in all cases as a clear, single-peak anomaly and it takes place at the expected temperature range as compared to vesicles in bulk by calorimetric measurements [29,56,57]. In some cases, a second maximum deviating from the linear, regular behaviour, can be observed at lower temperatures, which we ascribe to the pretransition. The appearance of this maximum will be discussed later. In order to obtain a more quantitative picture of temperature and size effects on the main phase transition, relevant parameters such as the area below the peak, the height of the maximum, peak width at half maximum, $\Delta T_{1/2}$, and the transition temperature (temperature corresponding to the peak maximum) have been extracted in

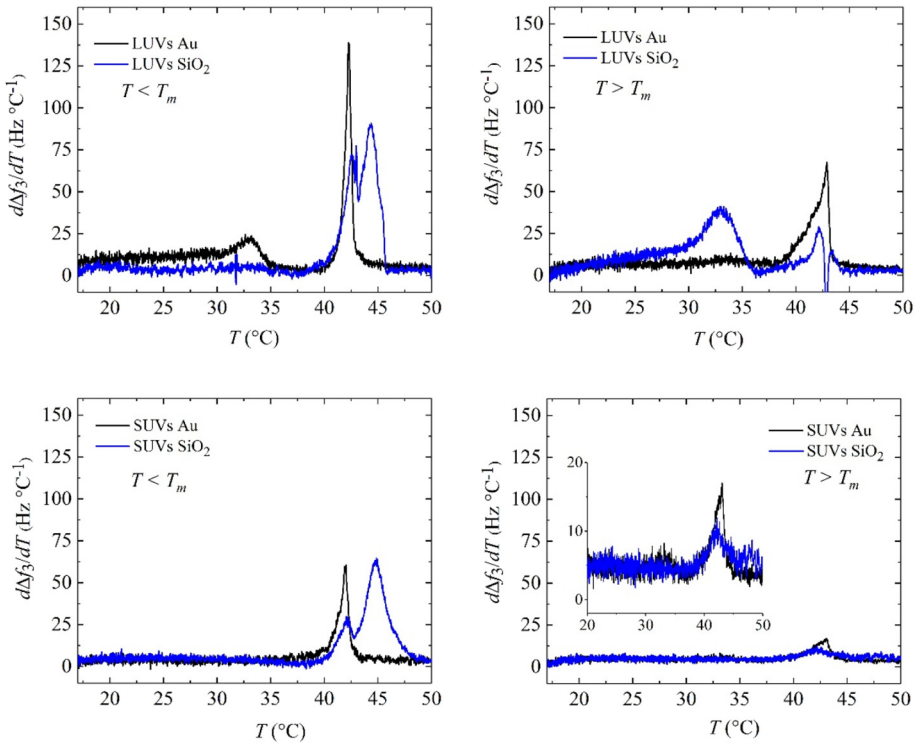

Fig. 6. Temperature dependence of $d\Delta f/dT$ (3rd overtone) for LUVs and SUVs adsorbed at $T > T_m$ and $T < T_m$ on Au- and SiO2-coated quartz surfaces. Black colour refers to supported membranes formed on Au and blue colour to supported membranes formed on SiO_2. The inset at the bottom right panel shows a magnification of the peak for clarity.

each case and are displayed in Fig. 7. It is observed that the size of the peak, as well as the area below scale with effective vesicle size. Large adsorbed vesicles carry more trapped aqueous buffer and are more deformable structures, thus, stronger changes in Δf and ΔD occur along the main transition. First-order derivatives of the dissipation can be found in Fig. S2 of the Supplementary material. The width of the

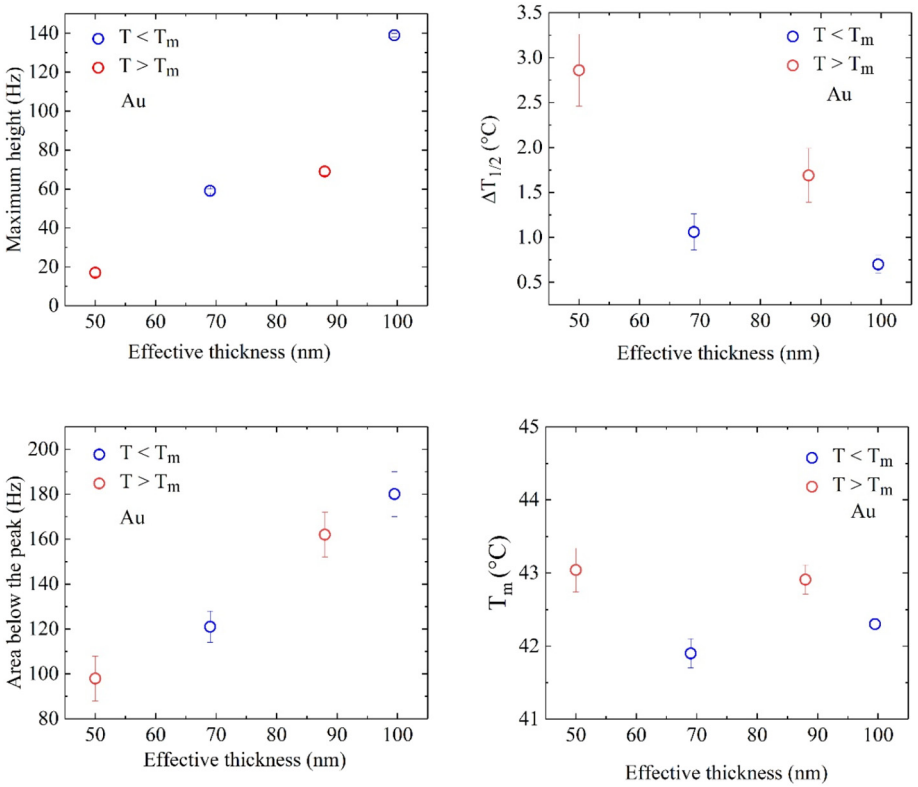

Fig. 7. Dependence of the main phase transition parameters on the effective thickness of adsorbed vesicles on Au-coated quartz surfaces. Blue colour refers to supported membranes adsorbed at $T > T_m$, while the red colour to membranes adsorbed at $T < T_m$.

peak at half maximum is related to the cooperativity of the transition, i.e., measure of the degree of intermolecular cooperation during the main transition. $\Delta T_{1/2}$ decreases as the size of the adsorbed vesicle layer, indicating that the melting takes place in a narrower temperature range as adsorbed vesicles deform less on the solid surface. $\Delta T_{1/2}$ increases as size decreases to a greater extent when vesicles are adsorbed $T > T_m$. For vesicles adsorbed at $T < T_m$ where deformation is very small, the transition temperature T_m shifts to lower values when decreasing size, since the higher curvature in SUVs decreases the lateral pressure [29,58]. In addition, adsorbed layers of LUVs might be a combination of mostly unilamellar and some oligolamellar vesicles. Lamellarity results in increased cooperativity during the membrane melting owing to the strengthened bilayer-bilayer interactions [59]. In general, the T_m values fall within the expected temperature range, although they are slightly higher than those observed for multilamellar vesicles (MLVs) and LUVs given the rather fast scanning rate (0.4 °C/min). At $T > T_m$, the extent of vesicle deformation is larger, they lie closer to the surface, presumably because of the decreased reduced volume v (see Fig. 5) and interactions with the substrate broaden the transition and increase the transition temperature.

3.3.2. Main phase transition of SVLs and SLBs on SiO_2 surfaces

Before analysing the phase transition behaviour, let us first recall the type of layers formed on SiO_2 surfaces. At $T < T_m$, DPPC vesicles were adsorbed and deformed to a larger extent as compared to Au; however, no global rupture and thus no SLB formation was observed. At $T > T_m$, both LUVs and SUVs are adsorbed, fused and ruptured to formed SLBs. As it can be observed in Fig. 6, the phase transition behaviour of these layers is greatly affected by the strong interactions between SiO_2 and the vesicles, resulting into films lying closer to the surface. For SVLs formed at $T < T_m$, the transition is greatly broadened and takes place in a double-peak manner. Fig. 8 presents a closer view on the double peak melting anomaly. Both peaks have been fitted to Gaussians in an effort to decouple their relative sizes. Decoupling effects have been experimentally observed for SLBs and double SLBs using AFM [60,61], DSC [62], neutron reflectometry [63] and single particle tracking [64]. They are ascribed to the stronger interaction between the lipid head groups of the proximal leaflet and the solid surface inducing a more tightly packed lipid distribution [31–33], which may favour the gel phase of lipids in the adhered part of the vesicle membrane [33] and/or the highly confined and orientationally ordered water layer between the proximal leaflet and the solid surface [31,32]. As a matter of fact, the viscosity of the interfacial water layer is 10^4 times larger than bulk water [64].

In the present work, apart from in DPPC SLBs on SiO_2, we also observe two peaks in the transitions of DPPC SVLs formed on SiO_2. For the latter, the double peak is attributed to a decoupling effect in the melting between the lower part of the vesicle that is closer to the surface and the upper part at the vesicle-buffer interface. The low temperature peak takes place at a similar temperature to the melting of vesicles adsorbed on Au (T_m ~ 42 °C). Hence, it confirms that this anomaly corresponds to the part of the vesicle envelope which is less affected by the solid surface.

The global size of both peaks scales with the effective adsorbed vesicle layer thickness. The individual peak sizes at the third overtone show an opposite pattern of behaviour between SVLs and SLBs. For SVLs on SiO_2 are greatly deformed and a large part of their area is in contact with the surface, while the remaining part melts like in bulk. As we shall see in the following section, SVLs formed on SiO_2 are quite unstable upon thermal cycling due to their largely deformed shape. In SLBs the peaks are less pronounced than in SVLs since the former are thinner and stiffer layers. Figs. S3 to S6 in the Supplementary material provide a complete overview of the transitions observed for all the systems in terms of frequency and dissipation at two overtones. The peak shapes show a complex behaviour for SLBs formed from LUVs owing to the fact that these layers might be a combination of multilayers and single bilayers. SLBs formed from SUVs precursors should be mostly single bilayers and show double peaks which are significantly broad. We aim to

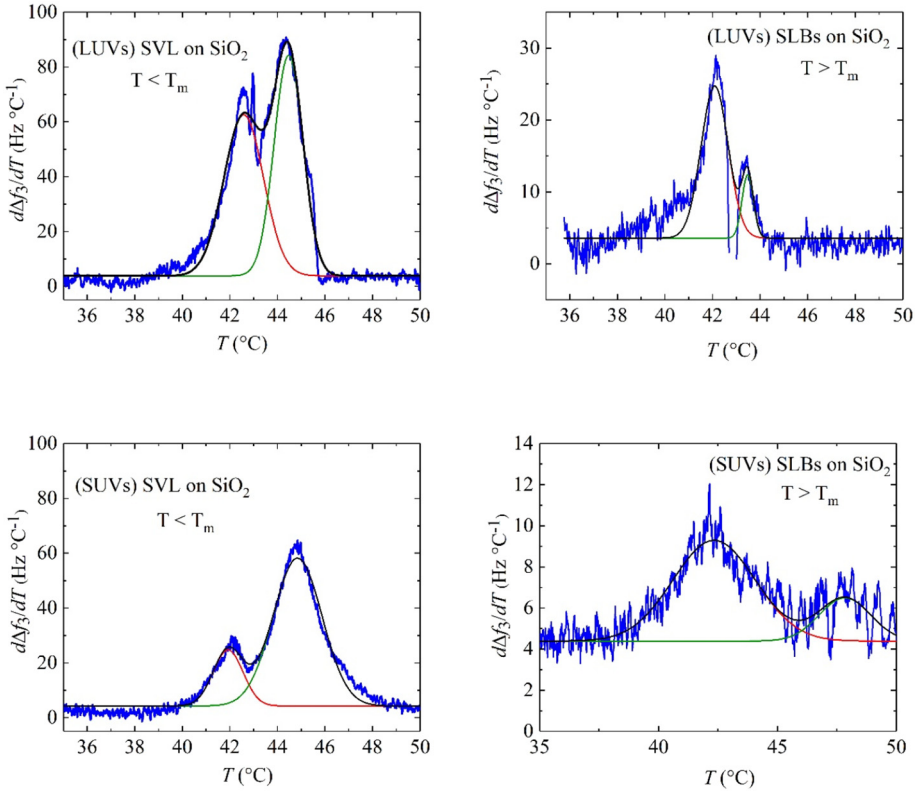

Fig. 8. Close view of the temperature dependence of $d\Delta f/dT$ (3rd overtone) for SVLs and SLBs formed from precursor LUVs and SUVs adsorbed at $T > T_m$ and $T < T_m$ on SiO2-coated quartz surfaces. Black, red and green solid lines correspond to gaussian multiple peak fitting results.

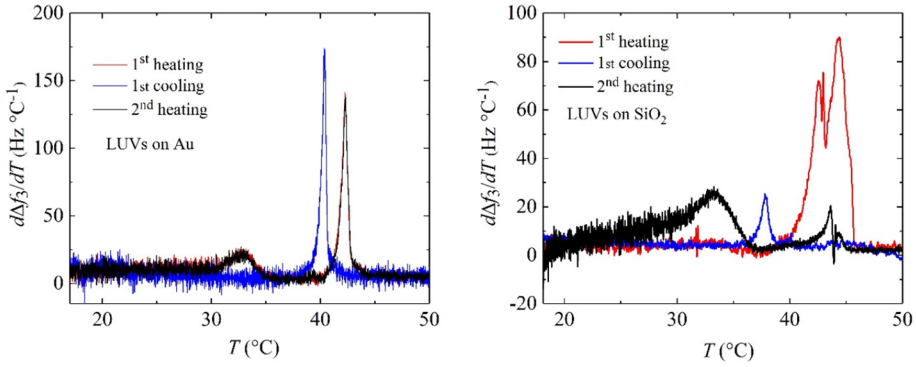

Fig. 9. $d\Delta f_3/dT$ vs temperature for the 3rd overtone upon successive heating and cooling runs for large DPPC vesicles adsorbed at $T < T_m$. Left panel: LUVs adsorbed on Au, right panel: LUVs adsorbed on SiO_2.

further explore the shapes of these two peaks in a follow up work by carrying out a purely systematic work.

3.3.3. Reversibility of the main transition and the pretransition

The stability of the main transition upon successive heating and cooling cycles has been also investigated. Fig. 9 displays an example of the $d\Delta f_3/dT$ temperature dependence for LUVs adsorbed at $T < T_m$ onto Au and SiO_2 surfaces. When adsorbed on Au, the main transition is fully reversible upon heating and cooling exhibiting a hysteresis of ~2 °C; this is reasonable considering the relatively fast scanning rate (0.4 °C/min) [65] as well as the first-order character of the transition. On the contrary, when adsorbed on SiO_2 LUVs exhibit irreversible changes. Upon cooling, a very large hysteresis occurs and the main transition takes place as a single peak. Upon the second heating, the frequency derivative resembles the one observed for SLBs on SiO_2 formed from LUVs adsorbed at $T < T_m$ (see Fig. 6, right column, upper panel). The additional thermal cycling on already deformed SVLs on SiO_2 induced rupture of the vesicles forming SLBs. This indicates that vesicles adsorbed on SiO_2 are less stable. Figs. S7 to S9 in the Supplementary material show the transitions upon thermal cycling for the remaining systems. Transitions of SVLs on Au are fully reversible, independently of the adsorption temperature and the size of the precursor vesicles. When formed onto SiO_2, transitions are reversible for SLBs formed at $T > T_m$, while SVLs formed from SUVs at $T < T_m$ display irreversible changes.

In some cases, a broader transition at lower temperatures, attributed to the pretransition, is observed upon heating (see Fig. 6). The pretransition typically takes place between the ripple phase and the liquid-disordered phase, the former being linked to the formation of periodic ripples on the membrane surface [66]. Ripples with periodicity ranging from 12 nm to 16 nm appear along the so-called stable ripple phase [67], subject to variations as a function hydration and thermal history [68–70]. The stable ripple phase is formed upon heating the sample from the gel phase to the liquid phase; a metastable ripple phase typically appears on cooling from the liquid crystalline phase to the gel phase [70]. From a biological viewing point, pretransition attracts interest arising from its potential to drive the membrane protein assembly via the so-called 'orderphobic' effect [71]. The question whether the pretransition takes place in solid-supported small vesicles has not been yet clearly answered; note that its existence could be hampered by enhanced curvature or even by the presence of the solid support. Its study on solid-supported membranes is limited to AFM measurements of lipid multilayers [72] and SLBs [73–75]. For single phospholipid SLBs, the formation of ripples is precluded due to lateral stress from the solid substrate, while in the presence of tris(hydroxymethyl) aminomethane (Tris) in a buffer solution, the ripples reappear [73]. The mechanisms behind this phenomenon are not fully understood. To our knowledge, the pretransition in small solid-supported vesicles is restricted to systems supported on silica beads by differential scanning calorimetry [76], where no pretransition could be observed. In our experiments, when the formed layers are intact vesicles, the transition is more clearly visible for LUVs. The latter, as explained above, are a combination of mostly unilamellar and few oligolamellar structures and possess enough free area for the pre-transition to take place. Small vesicles are mostly unilamellar and in the absence of lamellar stacks (geometrical constraints) the pretransition is expected to be weaker and overlap with the main transition, which is already shifted towards lower temperatures for small vesicles [29]. For SLBs, the pretransition is very clear for those formed from adsorbed LUVs that ruptured into thin rigid layers. It is thus tempting to state that, despite being rigid and thin, those SLBs consist of several bilayers (multilamellar) where the pretransition can take place and be detectable.

Unlike the main transition, the pretransition is not detected upon cooling. The irreversibility of the pretransition has been observed by Tenchov et al. using time-resolved X-ray diffraction [77]. After reaching the liquid disordered phase upon heating, the formation of ripples upon the following cooling might be strongly hindered and require a very long time, thus undercooling occurs.

4. Conclusions

We have examined the adhesion and phase behaviour of DPPC vesicles onto two types of surfaces, SiO_2 and Au bearing different adhesion levels. Relevant parameters associated with vesicle adhesion, such as vesicle radius and bending modulus, were also varied.

On a given surface, vesicle deformation is promoted for large vesicles at temperatures above their melting (small bending modulus). SiO_2-adsorbed vesicles deform to a greater extent than their counterparts on Au, resulting in higher contact area and higher membrane lateral tension, making them more prone to pore formation or rupture and fusion. Numerical calculations based on free energy minimization illustrate the interplay of bending and adhesion contributions into the vesicle shapes of different sizes and bending modulus on surfaces bearing different degrees of adhesion.

The temperature derivatives $d\Delta f/dT$ and $d\Delta D/dT$ show clear signatures of the phase transitions during heating and cooling runs. The main transition is reversible and the transition peak size scales with vesicle size. When adsorbed on Au at $T < T_m$, larger vesicles display a more cooperative transition, whereas the transition temperature T_m shifts downwards for smaller vesicles, reflecting that a larger curvature decreases the lateral pressure. At $T > T_m$, the extent of vesicle deformation is larger, the interactions with the substrate broaden the transition and increase the transition temperature. When adsorbed onto SiO_2 the main transition is greatly broadened and appears as a double-peak anomaly. The peak size appears larger for intact vesicles than for planar bilayers. The double peak can be explained as a decoupling effect in the melting

between the lower part of the membrane that is closer to the surface and the upper part at the membrane-buffer interface. The stronger interaction between the lipid head groups of the proximal leaflet and the solid surface induces a more tightly packed lipid distribution. This combined with the highly confined and orientationally ordered water layer make the adhered part of the membrane melt at a higher temperature than in bulk.

Supported DPPC vesicles are stable on Au and display fully reversible transitions irrespective of the adsorption temperature and the size of the precursor vesicles. Conversely, adhered vesicles onto SiO_2 are less stable and display irreversible changes upon thermal cycling. The low temperature between the gel and the ripple phase is clearly detectable for large adsorbed vesicles and from supported lipid bilayers obtained from the rupture of large vesicles. For the latter some degree of oligolamellarity is still present favouring the pretransition.

This work paves the way for studying the interplay of elastic and adhesive contributions of adsorbed lipid vesicles in more complex systems (by varying the lipid composition, surface charge, buffer ionic strength) and processes with different membrane geometries where the phase and size of vesicles are relevant parameters (vesicle-vesicle and vesicle-planar bilayer lipid exchange and fusion). It can also be extended to study the phase behaviour in the presence of external factors (peptide phase stabilization) and explore transitions close to non-equilibrium states.

CRediT authorship contribution statement

N. Bibissidis: Data acquisition and analysis, **K. Betlem**: Data acquisition, **G. Cordoyiannis**: Methodology, data analysis, writing, reviewing and editing, **F. Prista-von Bonhorst**: Data acquisition, **J. Goole**: Data acquisition and methodology, **J. Raval, M. Daniel**: Numerical calculations, **W. Góźdź**: Numerical calculations and fund raising, **A. Iglič**: Conceptualization, writing, reviewing, editing and fund raising, **P. Losada-Pérez**: conceptualization, supervision, writing, reviewing, editing and fund raising.

Declaration of competing interest

The authors declare no conflict of interest.

Acknowledgements

P.L.P. and K.B. acknowledge funding of the projects 'SADI' n 20061 y the programme Action Recherche Concertée, Université Libre de Bruxelles (ULB) and SurfTBiomem project n. F.4525.20 by the 'Fonds de la Recherche Scientifique' (FNRS). G.C. acknowledges the financial support of the Project CZ.02.2.69/0.0/0.0/16_027/0008465 for Mobility of Researchers under the Operational Programme Research, Development and Education. J.R. and W.G. acknowledge funding from the European Union's Horizon 2020 - Research and Innovation Framework Programme under the H2020 Marie Skłodowska-Curie Actions grant agreement No. 711859 and scientific work funded from the financial resources for science in the years 2017–2021 awarded by the Polish Ministry of Science and Higher Education for the implementation of an international co-financed project. A.I. acknowledges the support from Slovenian Research Agency (ARRS) through programme No. P2-0232 and the funding from the European Union's Horizon 2020 - Research and Innovation Framework Programme under grant agreement No. 801338 (VES4US project).

Appendix A. Supplementary data

Supplementary data to this article can be found online at https://doi.org/10.1016/j.molliq.2020.114492.

References

[1] P. Walde, Building artificial cells and protocell models: experimental approaches with lipid vesicles, BioEssays 32 (2010) 296–303, https://doi.org/10.1002/bies.200900141.
[2] Y. Xia, C. Xu, X. Zhang, P. Ning, Z. Wang, J. Tian, X. Chen, Liposome-based probe for molecular imaging: from basic research to the bedside, Nanoscale 11 (2019) 5822–5838, https://doi.org/10.1039/C9NR00207C.
[3] V. Noireaux, A. Libchaber, A vesicle bioreactor as a step toward an artificial cell assembly, Proc. Natl. Acad. Sci. 101 (2004) 17669–17674, https://doi.org/10.1073/pnas.0408236101.
[4] A. Sahmad, Y. Sultana, M. Aqil, Liposomal drug delivery systems: an update review, Curr. Drug Deliv. 4 (2007) 297–305, https://doi.org/10.2174/156720107782151269.
[5] Q. Liu, B.J. Boyd, Liposomes in biosensors, Analyst 138 (2013) 391–409, https://doi.org/10.1039/c2an36140j.
[6] R. Lipowsky, U. Seifert, Adhesion of vesicles and membranes, Mol. Cryst. Liq. Cryst. 202 (1991) 17–25, https://doi.org/10.1080/00268949108035656.
[7] J.H. Hurley, E. Boura, L.A. Carlson, B. Rózycki, Membrane budding, Cell 143 (2010) 875–887, https://doi.org/10.1016/j.cell.2010.11.030.
[8] S.R. Tabaei, J.J.J. Gillisen, S. Vafaei, J.T. Groves, N.J. Cho, Size-dependent, stochastic nature of lipid exchange between nano-vesicles and model membranes, Nanoscale 8 (2016) 13513–13520, https://doi.org/10.1039/c6nr03817d.
[9] M. Colombo, G. Raposo, C. Théry, Biogenesis, secretion, and intercelular interactions of exosomes and other extracellular vesicles, Annu. Rev. Cell Dev. Biol. 30 (2014) 255–289, https://doi.org/10.1146/annurev-cellbio-101512-122326.
[10] M. Yáñez-Mó, et al., Biological properties of extracellular vesicles and their physiological functions, J. Extracell. Vesicles 4 (2015) 27066, https://doi.org/10.3402/jev.v4.27066.
[11] H.J. Deuling, W. Helfrich, The curvature elasticity of fluid membranes: a catalogue of vesicle shapes, J. Phys. 37 (1976) 1335–1345, https://doi.org/10.1051/jphys:019760037011013350.
[12] L. Hirst, P. Uppamoochikkal, C. Lor, Phase separation and critical phenomena in biomimetic ternary lipid mixtures, Liq. Cryst. 38 (2011) 1735–1747, https://doi.org/10.1080/02678292.2011.615947.
[13] T. Hianik, V.I. Passechnik, Bilayer Lipid Membranes: Structure and Mechanical Properties, Kluwer Academic, Dordrecht, 1995.
[14] R.L. Biltonen, A statistical-thermodynamic view of cooperative structural changes in phospholipid bilayer membranes: their potential role in biological function, J. Chem. Thermodyn. 220 (1990) 1–19, https://doi.org/10.1016/0021-9614(90)90026-M.
[15] T. Muzic, F. Tounsi, S.B. Madsen, D. Pollakowski, M. Konrad, T. Heimburg, Melting transitions in biomembranes, Biophys. Biochim. Acta 1861 (2019), 183026, https://doi.org/10.1016/j.bbamem.2019.07.014.
[16] H.I. Kantor, S. Mabrey, J.H. Prestegard, J.M. Stutervant, Calorimetric examination of stable and fusing lipid bilayer vesicles, Biochim. Biophys. Acta 466 (1977) 402–410, https://doi.org/10.1016/0005-2736(77)90333-9.
[17] B.R. Lentz, T.J. Carpenter, D.R. Alford, Spontaneous fusion of phosphatidylcholine small unilamellar vesicles in the fluid phase, Biochemistry 26 (1987) 5389–5397, https://doi.org/10.1021/bi00391a026.
[18] S. Neupane, Y. De Smet, F.U. Renner, P. Losada-Pérez, Quartz crystal microbalance with dissipation monitoring: a versatile tool to monitor phase transitions in biomimetic membranes, Front. Mater. 5 (2018) 1–8, https://doi.org/10.3389/fmats.2018.00046.
[19] I. Reviakine, D. Johannsmann, R.P. Richter, Hearing what you cannot see and visualizing what you hear: interpreting quartz crystal microbalance data from solvated interfaces, Anal. Chem. 83 (2011) 8838–8848, https://doi.org/10.1021/ac201778h.
[20] C.A. Keller, B. Kasemo, Surface specific kinetics of vesicle of vesicle adsorption by quartz crystal microbalance, Biophys. J. 75 (1998) 1397–1402, https://doi.org/10.1016/S0006-3495(98)74057-3.
[21] R. Richter, A. Mukhopadhyay, A. Brisson, Pathways of lipid vesicle deposition on solid surfaces: a combined QCM-D and AFM study, Biophys. J. 85 (2003) 3035–3047, https://doi.org/10.1016/S0006-3495(03)74722-5.
[22] N.J. Cho, C.W. Frank, B. Kasemo, F. Höök, Quartz crystal microbalance with dissipation monitoring of supported lipid bilayers on various substrates, Nat. Prot. 5 (2010) 1096–1106, https://doi.org/10.1038/nprot.2010.65.
[23] A. Mechler, S. Praporski, K. Atmuri, M. Boland, F. Separovic, L.L. Martin, Specific and selective peptide-membrane interactions revealed using quartz crystal microbalance, Biophys. J. 93 (2007) 3907–3916, https://doi.org/10.1529/biophysj.107.116525.
[24] P. Losada-Pérez, M. Khorshid, C. Hermans, T. Robijns, M. Peeters, K.L. Jiménez-Monroy, L.T.N. Truong, P. Wagner, Melittin disruption of raft and non-raft forming biomimetic membranes: a study by quartz crystal microbalance with dissipation monitoring, Colloids Surf. B Biointerfaces 123 (2014) 938–944, https://doi.org/10.1016/j.colsurfb.2014.10.048.
[25] S.K. Pramanik, S. Senneca, A. Ethirajan, S. Neupane, F.U. Renner, P. Losada-Pérez, Ionic strength dependent vesicle adsorption and phase behavior of anionic phospholipid on a gold substrate, Biointerphases 11 (2016) 019006.
[26] A. Peschel, A. Langhoff, E. Uhl, A. Dathathreyan, S. Haindl, D. Johannsmann, I. Reviakine, Lipid phase behavior studied with a quartz crystal microbalance: a technique for biophysical studies with applications in screening, J. Chem. Phys. 145 (2016), 204904, https://doi.org/10.1063/1.4968215.
[27] Y.H. Hasan, A. Mechler, Nanoviscosity measurements revealing domain formation in biomimetic membranes, Anal. Chem. 89 (2017) 1855–1862, https://doi.org/10.1021/acs.analchem.6b04256.
[28] S. Mabrey, J.M. Stutervant, Investigation of phase transitions of lipids and lipid mixtures by high sensitivity differential scanning calorimetry, Proc. Natl. Acad. Sci. 73 (1976) 3862–3866, https://doi.org/10.1073/pnas.73.11.3862.

[29] T. Heimburg, Thermal Biophysics of Membranes, Wiley-VCH Verlag GmbH, Weinheim, 2007.
[30] C.A.R. Chapman, H. Chen, M. Stamou, J. Biener, M.M. Biener, P.J. Lein, E. Seker, Nanoporous gold as neural interface coating: effects of topography surface chemistry and feature size, ACS Appl. Mater. Interfaces 7 (2015) 7093–7100, https://doi.org/10.1021/acsami.5b00410.
[31] A. Velikonja, P.B. Santhosh, E. Gongadze, M. Kulkarni, K. Eleršič, Š. Perutkova, V. Kralj-Iglič, N. Poklar Ulrih, A. Iglič, Interaction between dipolar lipid headgroups and charged nanoparticles mediated by water dipoles and ions, Int. J. Mol. Sci. 14 (2013) 15312–15329, https://doi.org/10.3390/ijms140815312.
[32] E. Gongadze, A. Velikonja, Š. Perutkova, P. Kramar, A. Maček-Lebar, V. Kralj-Iglič, A. Iglič, Ions and water molecules in an electrolyte solution in contact with charged and dipolar surfaces, Electrochim. Acta 126 (2014) 42–60, https://doi.org/10.1016/j.electacta.2013.07.147.
[33] T. Goršak, M. Drab, D. Križaj, M. Jeran, J. Genova, S. Kralj, D. Lisjak, V. Kralj-Iglič, A. Iglič, D. Makovec, Magneto-mechanical actuation of barium-hexaferrite nanoplatelets for the disruption of phospholipid membranes, J. Coll. Interface Sci. 579 (2020) 508–519.
[34] T.H. Anderson, Y. Min, K.L. Weirich, H. Zeng, D. Fygenson, J.N. Israelachvili, Formation of supported bilayers on silica substrates, Langmuir 25 (2009) 6997–7005, https://doi.org/10.1021/la900181c.
[35] R. Tero, Substrate effects on the formation process, structure and physicochemical properties of supported lipid bilayers, Materials 5 (2012) 2658–2680, https://doi.org/10.3390/ma5122658.
[36] D.K. Owens, R.C. Wendt, Estimation of the surface free energy of polymers, J. Appl. Polym. Sci. 13 (1969) 1741–1747, https://doi.org/10.1002/app.1969.070130815.
[37] V.P. Zhadov, K. Dimitrievski, B. Kasemo, Adsorption and spontaneous rupture of vesicles composed of two types of lipids, Langmuir 22 (2006) 3477–3480, https://doi.org/10.1021/la053163f.
[38] E. Tellechea, D. Johannsmann, N.F. Steinmetz, R.P. Richter, I. Reviakine, Model-independent analysis of QCM data on colloidal particle dispersion, Langmuir 25 (2009) 5177–5184, https://doi.org/10.1021/la803912p.
[39] P. Meleard, C. Gerbeaud, T. Pott, L. Fernández-Puente, I. Bivas, M.D. Mitov, J. Dufourcq, P. Bothorel, Bending elasticities of model membranes: influences of temperature of sterol content, Biophys. J. 72 (1997) 2616–2629.
[40] R.M. Raphael, R.E. Waugh, Accelerated interleaflet transport of phosphatidylcholine molecules in membranes under deformation, Biophys. J. 71 (1996) 1374–1388.
[41] T.K. Lind, M. Cárdenas, H.P. Wacklin, Formation of supported lipid bilayers by vesicle fusion – effect of deposition temperature, Langmuir 30 (2014) 7259–7263, https://doi.org/10.1021/la500897x.
[42] E. Reimhult, F. Höök, B. Kasemo, Vesicle adsorption on SiO_2 and TiO_2: dependence on vesicle size, J. Chem. Phys. 117 (2002) 7401–7404, https://doi.org/10.1063/1.1515320.
[43] R. Dimova, Membrane electroporation in high electric fields, in: R.C. Alkire, D.M. Kolb, J. Lipkowski (Eds.), Advances in Electrochemical Science and Engineering: Bioelectrochemistry, vol. 13, Wiley-VCH, Weinheim 2011, pp. 335–367, https://doi.org/10.1002/9783527644117.ch7.
[44] A.P. Serro, A. Carapeto, G. Paiva, J.P.S. Farinha, R. Colaço, B. Saramago, Formation of an intact liposome layer adsorbed on oxidized gold confirmed by three complementary techniques: QCM-D, AFM and confocal fluorescence microscopy, Surf. Interface Anal. 44 (2012) 426–433, https://doi.org/10.1002/sia.3820.
[45] J.P. Cloarec, C. Chevalier, J. Genest, J. Beauvais, H. Chamas, Y. Chevolot, T. Baron, A. Soui, pH driven addressing of silicon nanowires onto Si3N4/SiO2 micro-patterned surfaces, Nanotechnology 27 (2016) 295602, https://doi.org/10.1088/0957-4484/27/29/295602.
[46] F.L. Leite, C.C. Bueno, A.L. Da Róz, E.C. Ziemath, O.N. Oliveira Jr., Theoretical models for surface forces and adhesion and their measurement using atomic force microscopy, Int. J. Mol. Sci. 13 (2012) 12773–12856, https://doi.org/10.3390/ijms131012773.
[47] W. Rawicz, K.C. Olbrich, T. McIntosh, D. Needham, E. Evans, Effect of chain length and unsaturation on elasticity of lipid bilayers, Biophys. J. 79 (2000) 328–339, https://doi.org/10.1016/S0006-3495(00)76295-3.
[48] I. Reviakine, M. Gallego, D. Johannsmann, E. Tellechea, Adsorbed liposome deformation studied by quartz crystal microbalance, J. Chem. Phys. 136 (2012), 084702, https://doi.org/10.1063/1.3687351.
[49] A.L.J. Olsson, I.R. Quevedo, D. He, M. Basnet, N. Tufenkji, Using the quartz crystal microbalance with dissipation monitoring to evaluate the size of nanoparticles deposited on solid surfaces, ACS Nano 7 (2013) 7833–7843, https://doi.org/10.1021/nn402758w.
[50] A.R. Fehran, J.A. Jackman, N.J. Cho, Investigating how vesicle size influences vesicle adsorption on titanium dioxide: a competition between steric packing and shape deformation, Phys. Chem. Chem. Phys. 19 (2017) 2131–2139, https://doi.org/10.1039/C6CP07930J.
[51] A. Iglič, V. Kralj-Iglič, J. Majhenc, Cylindrical shapes of closed lipid bilayer structures correspond to an extreme area difference between the two monolayers of the bilayer, J. Biomech. 32 (1999) 1343–1347, https://doi.org/10.1016/S0021-9290(99)00136-0.
[52] W.T. Góźdź, Spontaneous curvature induced shape transformations of tubular polymersomes, Langmuir 20 (2004) 7385–7391, https://doi.org/10.1021/la049776u.
[53] J. Steinkühler, J. Agudo-Canalejo, R. Lipowsky, R. Dimova, Modulating vesicle adhesion by electric fields, Biophys. J. 111 (2016) 1454–1464, https://doi.org/10.1016/j.bpj.2016.08.029.
[54] J.M. Holopainen, M.I. Angelova, P.K.J. Kinnunen, Vectorial budding of vesicles by asymmetrical enzymatic formation of ceramide in giant liposomes, Biophys. J. 78 (2000) 830–838.
[55] V. Kralj-Iglič, Stability of membranous nanostructures: a possible key mechanism in cancer progression, Int. J. Nanomedicine 7 (2012) 3579–3596, https://doi.org/10.2147/IJN.S29076.
[56] P. Losada-Pérez, K.L. Jiménez-Monroy, B. van Grinsven, J. Leys, S.D. Janssens, M. Peeters, C. Glorieux, J. Thoen, K. Haenen, W. De Ceuninck, P. Wagner, Phase transitions in lipid vesicles detected by a complementary set of methods: heat transfer measurements, adiabatic scanning calorimetry and dissipation-mode quartz crystal microbalance, Phys. Stat. Solidi A 211 (2014) 1377–1388, https://doi.org/10.1002/pssa.201431060.
[57] P. Losada-Pérez, N. Mertens, B. de Medio-Vasconcelos, E. Slenders, J. Leys, M. Peeters, B. van Grinsven, J. Gruber, C. Glorieux, H. Pfeiffer, P. Wagner, J. Thoen, Phase transitions of binary liquid mixtures: a combined study by adiabatic scanning calorimetry and quartz crystal microbalance with dissipation monitoring, Adv. Cond. Matter Phys. 2015 (2015) 479318, https://doi.org/10.1155/2015/479318.
[58] T. Brumm, K. Jorgensen, O.G. Mouritsen, T.M. Bayerl, The effect of increasing membrane curvature on the phase transition and mixing behaviour of dimirystoyl-sn-glycero-3-phosphatidylcholine/distearoyl-sn-glycero-3-phosphatidylcholine lipid mixture as studied by fourier transform infrared spectroscopy and differential scanning calorimetry, Biophys. J. 70 (1996) 1373–1379, https://doi.org/10.1016/S0006-3495(96)79695-9.
[59] J. Drazenovic, H. Wang, K. Roth, J. Zhang, S. Ahmed, Y. Chen, G. Bothun, S.L. Wunder, Effect of lamellarity and size on calorimetric phase transitions in single component phosphatidylcholine vesicles, Biochim. Biophys. Acta 1848 (2015) 532–543, https://doi.org/10.1016/j.bbamem.2014.10.003.
[60] D. Keller, N.B. Larsen, I.M. Møller, O.G. Mouritsen, Decoupled phase transitions and grain-boundary melting in supported phospholipid bilayers, Phys. Rev. Lett. 94 (2005), 025701, https://doi.org/10.1103/PhysRevLett.94.025701.
[61] Z.V. Feng, T.A. Spurlin, A.A. Gewirth, Direct visualization of asymmetric behavior in supported lipid bilayers at the gel-fluid phase transition, Biophys. J. 88 (2005) 2154–2164, https://doi.org/10.1529/biophysj.104.052456.
[62] J. Yang, J. Appleyard, The main transition in mica-supported phosphatidylcholine membranes, J. Phys. Chem. B 104 (2000) 8097–8100, https://doi.org/10.1021/jp001403o.
[63] Y. Gerelli, Phase transitions in a single supported phospholipid bilayer: real-time determination by neutron reflectometry, Phys. Rev. Lett. 122 (2019), 248101, https://doi.org/10.1103/PhysRevLett.122.248101.
[64] R.L. Schoch, I. Barel, F.L.H. Brown, G. Haran, Lipid diffusion in the distal and proximal leaflets of supported lipid bilayer membranes studied by single particle tracking, J. Chem. Phys. 148 (2018), 123333, https://doi.org/10.1063/1.5010341.
[65] G. Ohlsson, A. Tigerström, F. Höök, B. Kasemo, Phase transitions in adsorbed lipid vesicles measured using a quartz crystal microbalance with dissipation monitoring, Soft Matter 7 (2011), 10749, https://doi.org/10.1039/C1SM05923H.
[66] T. Heimburg, A model for the lipid pretransition: coupling of ripple formation with the chain-melting transition, Biophys. J. 78 (2000) 1154–1165, https://doi.org/10.1016/S0006-3495(00)76673-2.
[67] U. Bernchou, H. Midtiby, J.H. Ipsen, A.C. Simonsen, Correlation between the ripple phase and stripe domains in membranes, Biochim. Biophys. Acta 1808 (2011) 2849–2858, https://doi.org/10.1016/j.bbamem.2011.08.023.
[68] J.A.N. Zasadzinski, Effect of stereoconfiguration on ripple phases ($P_{\beta'}$) of dipalmitoylphosphatidylcholine, Biochim. Biophys. Acta 946 (1988) 235–243, https://doi.org/10.1016/0005-2736(88)90398-7.
[69] K. Sengupta, V.A. Raghunathan, J. Katsaras, Novel structural features of the ripple phase of phospholipids, Europhys. Lett. 49 (2000) 722–728, https://doi.org/10.1209/epl/i2000-00210-x.
[70] J.W. Jones, L. Lue, A. Saiani, G.J.T. Tiddy, Density measurements through the gel and lamellar phase transitions of di-tetradecanoyl- and di-hexadecanoyl- phosphatidylcholines: observation of slow relaxation processes and mechanisms of phase transitions, Liq. Cryst. 32 (2005) 1465–1481, https://doi.org/10.1080/02678290500252196.
[71] S. Katira, K.K. Mandadapu, S. Vaikuntanathan, B. Smit, D. Chandler, Pre-transition effects mediate forces of assembly between transmembrane proteins, eLife 5 (2016) e13150, https://doi.org/10.7554/eLife.13150.
[72] Y. Fang, J. Yang, Role of the bilayer-bilayer interaction on the ripple structure of supported bilayers in solution, J. Phys. Chem. 100 (1996) 15614–15619, https://doi.org/10.1021/jp961054r.
[73] J.X. Mou, J. Yang, Z.F. Shao, Tris(hydroxymethyl)aminomethane (C4H11NO3) induced a ripple phase in supported unilamellar phospholipid bilayers, Biochemistry 33 (1994) 4439–4443, https://doi.org/10.1021/bi00181a001.
[74] H. Takahashi, A. Miyagi, L. Redondo-Morata, S. Scheuring, Temperature-controlled high speed AFM: real-time observation of ripple phase transitions, Small 12 (2016) 6106–6113, https://doi.org/10.1002/smll.201601549.
[75] M. Majewska, D. Mrdenovic, I.S. Pieta, R. Nowakowski, P. Pieta, Nanomechanical characterization of single phospholipid bilayer in ripple phase with PF-QNM AFM, Biochim. Biophys. Acta Biomembr. 1862 (2020), 183347, https://doi.org/10.1016/j.bbamem.2020.183347.
[76] C. Naumann, T. Brumm, T.M. Bayerl, Phase transition behavior of single phosphatidylcholine bilayers on a solid spherical support studied by DSC, NMR and FT-IR, Biophys. J. 63 (1992) 1314–1319, https://doi.org/10.1016/S0006-3495(92)81708-3.
[77] B.G. Tenchov, H. Yao, I. Hatta, Time-resolved X-ray diffraction and calorimetric studies at low scan rates. I. Fully hydrated dipalmitoylphosphatidylcholine (DPPC) and DPPC/water/ethanol phases, Biophys. J. 56 (1989) 758, https://doi.org/10.1016/S0006-3495(89)82723-7.